

Abstract

We show that in the tropics, tropical atmospheric dynamics force the subcloud moist static energy (MSE) over land and ocean to be very similar in, and only in, regions of deep convection. Using observed rainfall as a proxy for convection and reanalysis data to calculate MSE, we show that subcloud MSE in the non-convective regions may differ substantially between land and ocean but is uniform across latitudes in convective regions even on a daily timescale. This result holds also in CMIP5 model simulations of past cold and future warm climates. Furthermore, the distribution of rainfall amount in subcloud MSE is very similar over land and ocean with the peak at 343 J/g and a half width at half maximum of 3 J/g. As a result, the annual-maximum subcloud MSE at each location over land and ocean is subject to a common upper bound set by the convective regions.

Plain Language Summary

An extremely idealized picture of the tropical atmospheric dynamics is that deep convection sets a horizontally uniform free tropospheric troposphere profile. Here, we show that despite the idealization, this simple picture is very useful in explaining the observations; Convection occurs at very similar spatially uniform subcloud MSE regardless of over land or ocean.

1 Introduction

The tropics show, even at equal latitudes and despite a relatively uniform annual mean insolation, a large variety of local climates ranging from regions with highest rainfall globally to deserts. Given the paramount importance of rainfall over land for ecosystems and humans, the processes governing its distribution and how it may change in the future are focus of intense efforts both in terms of improved process representations in numerical climate models, and development of theories to interpret observations and model results (e.g., Lintner & Chiang, 2005; Seneviratne et al., 2013; Pendergrass et al., 2017; Byrne & O’Gorman, 2015). Understanding climate over land inevitably requires understanding its connection to the oceans. A fundamental difference between land and ocean is that over land, evapotranspiration is constrained by available moisture and, as a consequence, sensible heat flux plays a larger role over land than ocean. An important corol-

44 lary of this surface energy budget consideration that is robustly observed in global cli-
45 mate model simulations is that the surface temperature response to radiative forcing is
46 larger over land than ocean (Manabe et al., 1991).

47 The limited evaporation over land not only affects the partitioning between sen-
48 sible and latent heat flux, but also leads to different temperature lapse rates in the lower
49 layers of the troposphere over land and ocean. Joshi et al. (2008) note that in model cal-
50 culations there exists a level sufficiently high up in the troposphere where temperature
51 change in response to forcing is similar over land and ocean, and the larger surface tem-
52 perature response over land then is consistent with the different changes in lapse rates
53 over land and ocean. Byrne and O’Gorman (2013a) formulate this effect in terms of the
54 equality of equivalent potential temperature averaged over land and ocean as a result
55 of weak temperature gradients in the free troposphere and convective quasi-equilibrium,
56 which is largely supported by simulations with idealized climate models. However, they
57 also notice that this equality breaks down in realistic climate models (Byrne & O’Gorman,
58 2013b), and the changes in the mean surface equivalent potential temperature, rather
59 than the mean equivalent potential temperatures themselves, are more similar over land
60 and ocean (Byrne & O’Gorman, 2013b; Byrne & O’Gorman, 2018).

61 In the following, we present observation and model results to provide a more pre-
62 cise picture how tropical atmospheric dynamics couple the moist static static (MSE; equiv-
63 alent to the equivalent potential temperature used in (Byrne & O’Gorman, 2013a, 2013b))
64 of air near the surface over land and ocean to the free atmosphere. We show that the
65 subcloud MSE where convection occurs is roughly constant with latitude in the inner
66 tropics (about 20°S-20°N) and very similar over land and ocean, which may not be ex-
67 pected in light of the well-documented land-ocean contrast of tropical convection (Robinson
68 et al., 2011; Matsui et al., 2016). Notably, this similarity holds across all latitudes of the
69 inner tropics even on a daily timescale. As a result, the connection in subcloud MSE over
70 land and ocean is only established in the highest MSE values that compose the convective
71 regions.

2 Data and Method

2.1 Subcloud MSE

Subcloud MSE is computed using ERA-Interim 6-hourly reanalysis data on $0.75^\circ \times 0.75^\circ$ grid and pressure levels (Dee et al., 2011). Moist static energy h is calculated following the definition

$$h = c_p T + gz + Lq, \quad (1)$$

where c_p is the heat capacity of air, T is temperature, g is gravitational acceleration, z is height, L is the latent heat of water, and q is the mixing ratio of water vapor. Standard values used in climate models and reanalysis data are adopted here, namely $c_p = 1005 \text{ J/kg}$, $L = 2.5 \times 10^6 \text{ J/kg}$ and $g = 9.8 \text{ m/s}^2$. The subcloud layer is the portion of the boundary layer extending from the surface to the average altitude of the base of clouds (American Meteorological Society, 2012). Here, we calculate the lifting condensation level on 6-hourly time frequency. Subcloud MSE is then the average MSE either within the layer between the ground and the LCL when the LCL is within the boundary layer, or within the boundary layer when the LCL is higher than the boundary-layer top (no-cloud case). The 6-hourly subcloud MSE is averaged to a daily timescale to match the time resolution of the rainfall observation.

2.2 Convective subcloud MSE

The convective (subcloud) MSE is calculated by weighting the subcloud MSE in each grid box with the corresponding rainfall received, i.e., rainfall intensity multiplied by the area of the grid box, following the rainfall-weighting method in Flannaghan et al. (2014); Fueglistaler et al. (2015):

$$\text{Convective subcloud MSE} = \frac{\sum_i P_i h_i}{\sum_i P_i} \quad (2)$$

Daily rainfall observations from Tropical Rainfall Measuring Mission (TRMM) (Huffman et al., 2007) from 2001 to 2014 of $0.25^\circ \times 0.25^\circ$ resolution are interpolated to the ERA-Interim grid conserving total precipitation fluxes. The convective (subcloud) MSE can be loosely interpreted as the subcloud MSE weighted by the mass flux transported from the subcloud layer to the free atmosphere by deep convection, as convective mass flux scales roughly linearly with rainfall (Raymond et al., 2015). The resolution of the data used here (order 100 km) does not allow distinguishing between convective rain (1-10 km)

100 and stratiform rain (~ 100 km) (Houze, 1997), which may introduce some ambiguity in
101 the determination of convective MSE. For the convective MSE as a function of latitude,
102 the subcloud MSE in each latitude band is first calculated on a yearly basis before av-
103 eraged over the chosen period and hence is not influenced by trends or interannual vari-
104 ability in total tropical rainfall.

105 **3 Results**

106 **3.1 The MSE threshold for convection – A zeroth-order picture**

107 The tropical atmosphere can be seen as consisting of a boundary layer with diverse
108 temperature, humidity, and topography (the three components of MSE) and a free tro-
109 posphere that is comparatively homogenous. Deep convection transports boundary layer
110 air upward into the free atmosphere. Once the free atmosphere is filled with buoyant air
111 originating from the warm and humid boundary layer, it suppresses upward motion in
112 the colder regions, establishing a threshold for convection. More quantitatively, the con-
113 straint from atmospheric dynamics can be expressed as a combination of convective quasi-
114 equilibrium (QE) and weak temperature gradient (WTG) (Byrne & O’Gorman, 2013a),
115 subsequently referred to as QE-WTG. Strict quasi-equilibrium assumes that convection
116 maintains the subcloud MSE equal to the saturated MSE aloft in the free atmosphere
117 (e.g., Arakawa & Schubert, 1974; Emanuel, 2007) (The saturated MSE only strongly de-
118 pends on the air temperature). Weak temperature gradient states that the free atmo-
119 sphere cannot sustain substantial horizontal temperature gradients due to the smallness
120 of the Coriolis parameter in the tropics (e.g., Charney, 1963; A. H. Sobel & Bretherton,
121 2000). Consequently, at the limit of strict quasi-equilibrium and zero temperature gra-
122 dient, simultaneously convecting regions, regardless of over land or ocean, should have
123 the same subcloud MSE which we refer to as the MSE threshold for convection. While
124 previous studies (Byrne & O’Gorman, 2013a, 2013b; Byrne & O’Gorman, 2018) eval-
125 uate the QE-WTG picture with the large-scale mean MSE over land and ocean, we ar-
126 gue that QE-WTG should be evaluated only in the regions where deep convection cou-
127 ples the MSE in the subcloud layer to the free atmosphere and does not apply to the re-
128 gions where the subcloud MSE is too low to reach the threshold for convection. Lever-
129 aging the aforementioned rainfall-weighting method, we are able show that QE-WTG
130 apply to each latitude in the observations, even on a daily timescale, and there is a clear
131 breakdown of the theoretical picture around 20° in both hemispheres.

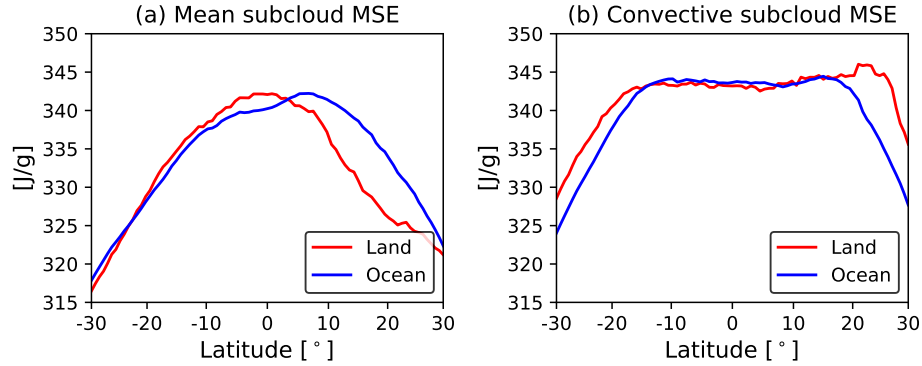


Figure 1. Zonal-mean (a) and convective (b) subcloud moist static energy (MSE) over land (red) and ocean (blue). Subcloud MSE is derived from ERA-Interim and rainfall is from TRMM. Daily data from 2001 to 2014 are used. The convective subcloud MSE is determined by weighting the subcloud MSE at each longitude with the corresponding rainfall within each latitudinal band of 0.75° wide.

132 The zonal-mean subcloud MSE (Fig. 1(a)) peaks around the equator reflecting the
 133 annual-mean solar forcing, whereas the convective subcloud MSE (Fig. 1(b)) is roughly
 134 uniform throughout the inner tropics and very similar between land and ocean, reflect-
 135 ing the weak horizontal temperature gradients in the free atmosphere. The sharp drop-
 136 off at about 20° in both hemispheres indicates where the Coriolis effect is no longer neg-
 137 ligible and QE-WTG breaks down. As a result, rainfall in the subtropics can occur ei-
 138 ther at very low subcloud MSE when induced by the extratropical eddies (Funatsu &
 139 Waugh, 2008) or at very high subcloud MSE during the South Asian monsoon which cre-
 140 ates the peak in the convective MSE around 25°N over land (Boos & Kuang, 2010). The
 141 contrast between the mean and the convective subcloud MSE resolves the aforementioned
 142 inconsistency between the strict QE-WTG theory and the realistic simulations mentioned
 143 in (Byrne & O’Gorman, 2013b); Convection only occurs in the part of the domain where
 144 the subcloud MSE is high enough to reach the tropically uniform MSE threshold of about
 145 343 J/g shown in Fig. 1(b), and in the part of the domain that is not convecting sub-
 146 cloud MSE is not coupled to the free atmosphere and therefore can differ between
 147 land and ocean.

148 A more stringent test examines how effectively QE-WTG works on a daily basis.
 149 Fig. 2 shows the seasonal evolution of the zonal-mean subcloud MSE in the convective

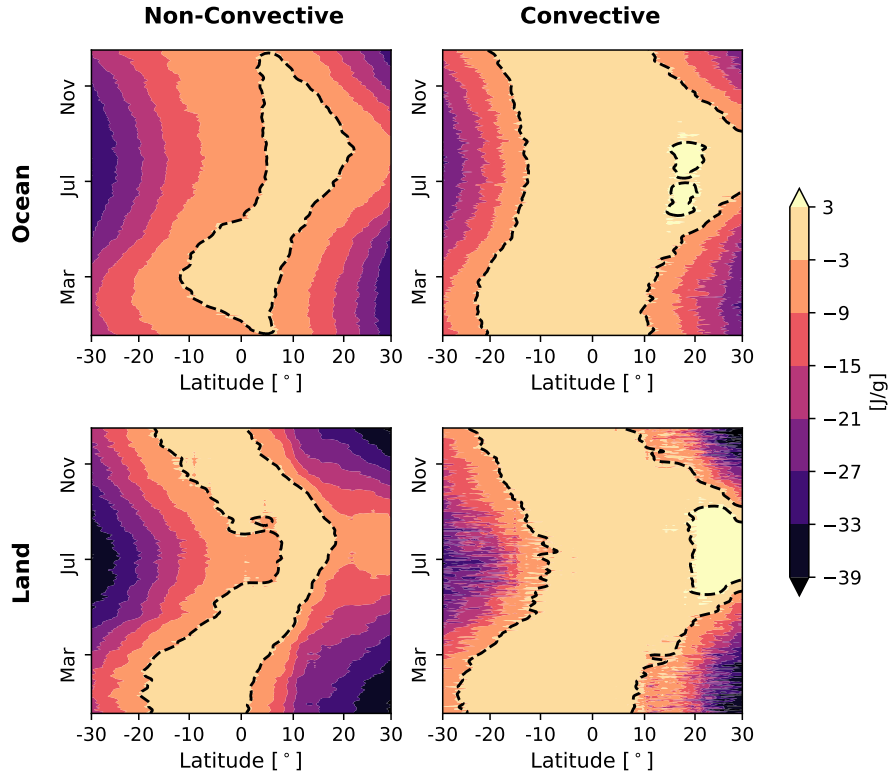


Figure 2. The mean subcloud moist static energy (MSE) as a function of latitude and day of year in the non-convective and convective regions over ocean and land. Daily data are used from ERA-Interim and TRMM between 2001 and 2014. Convective and non-convective regions are identified with a rainfall threshold of 6 mm/day. The dashed contour lines indicate the subcloud MSE within ± 3 J/g relative to a common reference value (see text).

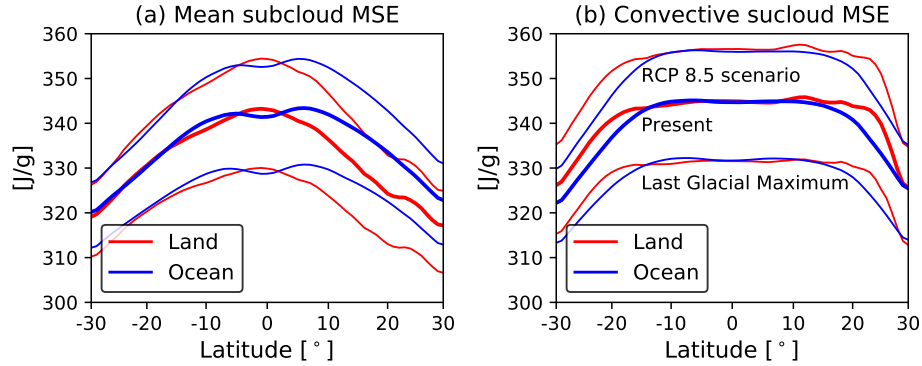


Figure 3. Zonal-mean (a) and convective (b) subcloud moist static energy (MSE) for model simulations. The multi-model mean of monthly data from CMIP5 models (See Table S1) are shown. Three experiments are shown from bottom to top: the Last Glacial Maximum, the period from 1979 to 2005 in the simulation of current climate (labeled “Present”), and the last 20 years of the 21st century in the global warming simulation (labeled “RCP 8.5 scenario”).

150 regions (left column) and non-convective regions (right column) over land (lower row)
 151 and ocean (upper row). Here the convective MSE is defined as the mean subcloud MSE
 152 where the rain rate is above 6 mm/day (A. Sobel et al., 2002) and *vice versa* for the non-
 153 convective MSE. The results are not sensitive to the choice of a rainfall threshold from
 154 2 mm/day to 20 mm/day (Figs. S1, S2). This method is different from the rainfall-weighting
 155 method used in Fig. 1 but yields similar convective MSE values, essentially because rain-
 156 fall anywhere in the inner tropics occurs at very similar subcloud MSE. To facilitate the
 157 comparison, a reference value for each day of year, calculated as the mean subcloud MSE
 158 in the convective regions over equatorial (5°S - 5°N) ocean, is subtracted. Even on a sin-
 159 gular day of year, the convective MSE is still uniform over a broad range in latitude, though
 160 this latitudinal range has seasonality (Fig. 2, right column). The seasonal evolution of
 161 the non-convective MSE has more prominent land-ocean contrast than the convective
 162 MSE (indicated by the shapes of the dashed black contours), supporting the concept that
 163 only the subcloud MSE in the convective regions over land and ocean are tied to the uni-
 164 form temperature in the free atmosphere.

165 The physics involved in the QE-WTG mechanism does not rely on the mean cli-
 166 matic state, therefore QE-WTG is expected to hold in all climates. Global climate mod-
 167 els from the Coupled Model Intercomparison Project phase 5 (CMIP5) (Taylor et al.,

168 2012) that correctly reproduce the observed uniform convective MSE in the simulations
 169 of the present climate (Fig. S3 and Table S1) also show a uniform convective MSE in
 170 the projections of a much warmer climate under the Representative Concentration Path-
 171 way 8.5 (RCP8.5) emission scenario (Fig. 3). Model simulations of the much colder Last
 172 Glacial Maximum also show a uniform convective MSE over both land and ocean. There-
 173 fore, Fig. 3 demonstrates the validity of QE-WTG in a wide range of climates.

174 **3.2 Finite width of the MSE threshold for convection – A first-order cor-** 175 **rection**

176 The latitudinal uniformity of the convective subcloud MSE in the inner tropics and
 177 its similarity between land and ocean (Fig. 1, 2) provide observational support for the
 178 zeroth-order picture. However, it is well established that factors such as the mid-tropospheric
 179 humidity (Emanuel, 2019; Brown & Zhang, 1997), convective inhibition (Mapes, 2000),
 180 low-level convergence (Lindzen & Nigam, 1987; Back & Bretherton, 2009), and station-
 181 ary or transient equatorial waves (Gill, 1980; Kiladis et al., 2009) all affect the trigger-
 182 ing of convection. How can these complicating factors be reconciled with the simple pic-
 183 ture of a uniform MSE threshold for convection?

184 The convective MSE threshold shown in Fig. 1(b) is a weighted mean over a range
 185 of subcloud MSE values rather than a single MSE value. Fig. 4(a) shows the total amount
 186 of rainfall that falls into each subcloud MSE bin of a width of 0.2 J/g . This rainfall dis-
 187 tribution can be roughly regarded as the convective mass flux distribution as a function
 188 of subcloud MSE. If QE-WTG were strict, this distribution would be a Dirac function
 189 at the highest subcloud MSE. In the observed climate, however, the majority of rainfall
 190 occurs around 343 J/g —the value is comparable to the convective MSE (Fig. 1(a))—with
 191 a Half Width at Half Maximum (HWHM) of 3 J/g . The half width of 3 J/g then encaps-
 192 ulates the previously mentioned factors that affect the local triggering of convection.
 193 This width is narrow compared to the entire range of the tropical subcloud MSE of about
 194 60 J/g . Remarkably, the shape of the rainfall distribution as a function of subcloud MSE
 195 is also similar between land and ocean, a result not predicted by the theoretical limit of
 196 QE-WTG.

197 The tails of the rainfall distribution at very high subcloud MSE above 350 J/g and
 198 low subcloud MSE below 336 J/g are somewhat different for land and ocean, due to the

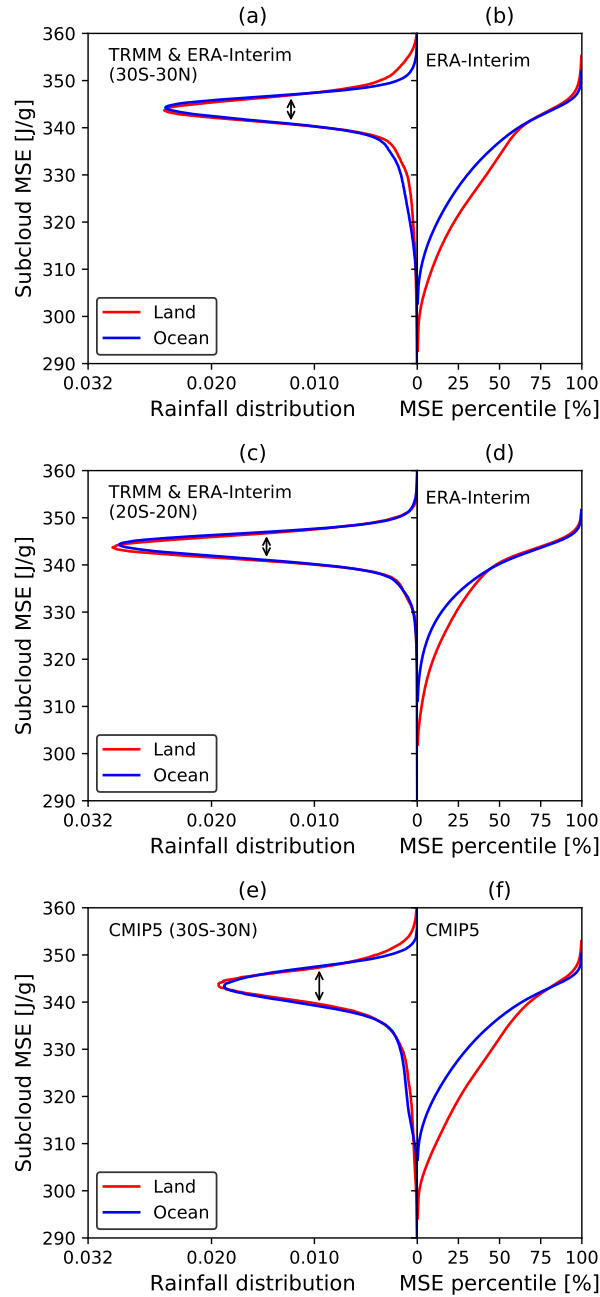


Figure 4. Rainfall distribution as a function of subcloud MSE (left panels) and the corresponding percentiles of subcloud MSE (right panels). (a) and (b) show rainfall from TRMM and subcloud MSE from ERA-Interim between 30°S and 30°N. (c) and (d) are the same as (a) and (b) but with data between 20°S and 20°N. (e) and (f) are the same as (a) and (b) but is the multi-model mean of monthly output from CMIP5 models in the coupled simulation from 1979 to 2005 (Table S1). The double arrows indicate where the HWHM is evaluated.

199 break-down of QE-WTG in the subtropics. When the latitudinal range is restricted to
 200 20°S-20°N (Fig. 4(c)), the tails disappear and a convective mode centered at 343 J/g emerges
 201 which is almost identical over land and ocean.

202 Fig. 4(e) is the same as Fig. 4(a) but for the CMIP5 multi-model mean. The width
 203 of the MSE threshold is wider than that in the observations, because it is an average of
 204 models with slightly different mean states. In fact, the half width for an individual CMIP5
 205 model is also 3 J/g on average.

206 To put the magnitude of the width into context, we compare it with typical MSE
 207 changes due to departure from the strict QE-WTG: Observed convective available po-
 208 tential energy (CAPE) varies between 0 and 4 J/g (Williams & Renno, 1993; Gettelman
 209 et al., 2002) and the free tropospheric temperature varies by order 1 K horizontally (e.g.
 210 Fueglistaler et al., 2009) which translates to about 2 J/g of subcloud MSE. It is thus not
 211 obvious which factor contributes more given the similar amplitudes. We also notice that
 212 the width is not strongly dependent on the time frequency (daily or monthly) of data.

213 Figs. 4(b,d,f) show the corresponding percentiles of subcloud MSE sorted in ascend-
 214 ing order and averaged in equal-area bins. Fig. 4(b) reiterates that only the highest sub-
 215 cloud MSE values between 30°S and 30°N are coupled over land and ocean while the low
 216 subcloud MSE values are free to differ – the upper 30% of subcloud MSE has almost iden-
 217 tical distribution over land and ocean while the lower 70% of the subcloud MSE over ocean
 218 is systematically higher than that over land. In addition, Figs. 4(b,d) highlight an in-
 219 teresting aspect of the Earth’s tropical climate: The convective area fraction is approx-
 220 imately equal over land and ocean.

221 4 Conclusion and outlook

222 We show that a simple theoretical picture of the tropical atmosphere based on the
 223 convective quasi-equilibrium and the weak-temperature-gradient assumptions (QE-WTG)
 224 can effectively explain the observations. In accordance with QE-WTG, the convective
 225 subcloud MSE is roughly constant with latitude between 20°S and 20°N on a daily timescale
 226 in the observed current climate and in the simulated past and future climates. The util-
 227 ity of QE-WTG is manifested in its capability of reconciling the land-ocean contrast. The
 228 vastly different land and ocean surfaces share almost identical convective subcloud MSE,
 229 distribution of highest subcloud MSE values, and precipitation distribution as a func-

230 tion of subcloud MSE. Whereas the role of subcloud MSE forcing the free troposphere
231 has been well appreciated in tropical convection, we demonstrate that the horizontally
232 uniform free tropospheric temperature forces the highest subcloud MSE values to be sim-
233 ilar over land and ocean, which is an interesting aspect of convection in the tropics. These
234 results fill the gap between the idealized, conceptual understanding of the tropical at-
235 mospheric dynamics and the real world consisting of diverse regional climates.

236 An important implication of our results is that the maximum subcloud MSE at a
237 given location, either over land or over ocean, is subject to a common upper bound set
238 by the convective regions. As moist static energy is related to heat stress metrics (Fischer
239 & Knutti, 2013; Sherwood & Huber, 2010; Byrne & O’Gorman, 2013b) and as is pointed
240 out in Byrne and O’Gorman (2013b) that the mean heat stress over land is controlled
241 by the ocean, our results suggest that atmospheric dynamics may also control heat stress
242 extremes in the tropics.

243 **Acknowledgments**

244 We thank Isaac Held and Nadir Jeevanjee for thoughtful feedback and discussion, and
245 Julius Busecke and Allison Hogikyan for suggestions on an earlier version of the manuscript.
246 Y.Z. acknowledges support from the Cooperative Institute for Modeling the Earth Sys-
247 tem (CIMES). S.F. acknowledges support from National Science Foundation Awards AGS-
248 1417659 and AGS-1743753. We acknowledge the European Centre for Medium-range Weather
249 Forecast (ECMWF) for providing ERA-Interim data ([https://www.ecmwf.int/en/forecasts/
250 datasets/archive-datasets/reanalysisdatasets/era-interim](https://www.ecmwf.int/en/forecasts/datasets/archive-datasets/reanalysisdatasets/era-interim)). We acknowledge
251 the National Aeronautics and Space Administration (NASA) for providing Tropical Rain-
252 fall Measuring Mission (TRMM) 3B42 data ([https://disc.gsfc.nasa.gov/datasets/
253 TRMM_3B42RT_Daily_V7/summary](https://disc.gsfc.nasa.gov/datasets/TRMM_3B42RT_Daily_V7/summary)). We acknowledge the World Climate Research Pro-
254 gramme’s Working Group on Coupled Modelling and climate modeling groups (Table
255 S1) for producing CMIP5 model data (<https://esgf-node.llnl.gov/projects/cmip5>).

256 **References**

- 257 American Meteorological Society. (2012). *Subcloud layer, glossary of meteorology*.
258 (http://glossary.ametsoc.org/wiki/Subcloud_layer, Last accessed on
259 2019-11-2)
- 260 Arakawa, A., & Schubert, W. H. (1974). Interaction of a cumulus cloud ensemble

- 261 with the large-scale environment, part i. *J. Atmos. Sci.*, *31*(3), 674–701.
- 262 Back, L., & Bretherton, C. (2009). On the relationship between sst gradients,
263 boundary layer winds, and convergence over the tropical oceans. *J. Climate*,
264 *22*, 4182–4196. doi: 10.1175/2009JCLI2392.1
- 265 Boos, W., & Kuang, Z. (2010). Dominant control of the south asian monsoon by
266 orographic insulation versus plateau heating. *Nature*, *463*, 218–222.
- 267 Brown, R. G., & Zhang, C. (1997). Variability of midtropospheric moisture and
268 its effect on cloud-top height distribution during toga coare. *J. Atmos. Sci.*,
269 *54*(23), 2760–2774.
- 270 Byrne, M. P., & O’Gorman, P. A. (2013a). Land–ocean warming contrast over
271 a wide range of climates: Convective quasi-equilibrium theory and idealized
272 simulations. *Journal of Climate*, *26*(12), 4000–4016.
- 273 Byrne, M. P., & O’Gorman, P. A. (2013b). Link between land-ocean warming
274 contrast and surface relative humidities in simulations with coupled climate
275 models. *Geophysical Research Letters*, *40*(19), 5223–5227.
- 276 Byrne, M. P., & O’Gorman, P. A. (2015). The response of precipitation minus evap-
277 otranspiration to climate warming: Why the “wet-get-wetter, dry-get-drier”
278 scaling does not hold over land. *Journal of Climate*, *28*(20), 8078–8092.
- 279 Byrne, M. P., & O’Gorman, P. A. (2018). Trends in continental temperature
280 and humidity directly linked to ocean warming. *Proceedings of the National*
281 *Academy of Sciences*, *115*(19), 4863–4868.
- 282 Charney, J. (1963). A note on large-scale motions in the tropics. *J. Atmos. Sci.*, *20*,
283 607–609.
- 284 Dee, D. P., Uppala, S., Simmons, A., Berrisford, P., Poli, P., Kobayashi, S., . . . oth-
285 ers (2011). The era-interim reanalysis: Configuration and performance of the
286 data assimilation system. *Quarterly Journal of the royal meteorological society*,
287 *137*(656), 553–597.
- 288 Emanuel, K. (2007). Quasi-equilibrium dynamics of the tropical atmosphere. *The*
289 *Global Circulation of the Atmosphere*, 186–218.
- 290 Emanuel, K. (2019). Inferences from simple models of slow, convectively coupled
291 processes. *J. Atmos. Sci.*, *76*(1), 195–208.
- 292 Fischer, E. M., & Knutti, R. (2013). Robust projections of combined humidity and
293 temperature extremes. *Nature Climate Change*, *3*(2), 126.

- 294 Flannaghan, T. J., Fueglistaler, S., Held, I. M., Po-Chedley, S., Wyman, B., & Zhao,
 295 M. (2014). Tropical temperature trends in Atmospheric General Circulation
 296 Model simulations and the impact of uncertainties in observed SSTs. *J.*
 297 *Geophys. Res.*, *119*(23), 13,327–13,337. doi: 10.1002/2014JD022365
- 298 Fueglistaler, S., Dessler, A. E., Dunkerton, T. J., Folkins, I., Fu, Q., & Mote,
 299 P. W. (2009). Tropical tropopause layer. *Rev. Geophys.*, *47*, RG1004. doi:
 300 10.1029/2008RG000267
- 301 Fueglistaler, S., Radley, C., & Held, I. M. (2015). The distribution of precipita-
 302 tion and the spread in tropical upper tropospheric temperature trends. *Geo-*
 303 *phys. Res. Letts.*, *42*(14), 6000-6007. doi: 10.1002/2015GL064966
- 304 Funatsu, B., & Waugh, D. (2008). Connections between potential vorticity intru-
 305 sions and convection in the eastern tropical pacific. *J. Atmos. Sci.*, *65*, 987–
 306 1002. doi: 10.1175/2007JAS2248.1
- 307 Gettelman, A., Seidel, D., Wheeler, M., & Ross, R. (2002). Multidecadal trends
 308 in tropical convective available potential energy. *J. Geophys. Res. Atmos.*,
 309 *107*(D21).
- 310 Gill, A. E. (1980). Some simple solutions for heat-induced tropical circulation. *Q. J.*
 311 *Roy. Meteor. Soc.*, *106*(449), 447–462.
- 312 Houze, R. (1997). Stratiform precipitation in regions of convection: A meteorological
 313 paradox? *Bulletin American Meteorological Society*, *78*(10), 2179–2196.
- 314 Huffman, G. J., Bolvin, D. T., Nelkin, E. J., Wolff, D. B., Adler, R. F., Gu, G., ...
 315 Stocker, E. F. (2007). The trmm multisatellite precipitation analysis (tmpa):
 316 Quasi-global, multiyear, combined-sensor precipitation estimates at fine scales.
 317 *Journal of hydrometeorology*, *8*(1), 38–55.
- 318 Joshi, M. M., Gregory, J. M., Webb, M. J., Sexton, D. M. H., & Johns, T. C.
 319 (2008). Mechanisms for the land/sea warming contrast exhibited by simu-
 320 lations of climate change. *Clim. Dynamics*, *30*, 455-465.
- 321 Kiladis, G. N., Wheeler, M., Haertel, P., Straub, K., & Roundy, P. (2009). Convec-
 322 tively coupled equatorial waves. *Rev. Geophys.*, *47*, RG2003. doi: 10.1029/
 323 2008RG000266
- 324 Lindzen, R., & Nigam, S. (1987). On the role of sea surface temperature gradients in
 325 forcing low-level winds and convergence in the tropics. *J. Atmos. Sci.*, *44*(17),
 326 2418–2436.

- 327 Lintner, B. R., & Chiang, J. C. (2005). Reorganization of tropical climate during
 328 el nino: A weak temperature gradient approach. *Journal of climate*, *18*(24),
 329 5312–5329.
- 330 Manabe, S., Stouffer, R., Spelman, M., & Bryan, K. (1991). Transient responses of a
 331 coupled ocean–atmosphere model to gradual changes of atmospheric co2. part
 332 i: Annual mean response. *J. Clim.*, *4*, 785–818.
- 333 Mapes, B. E. (2000). Convective inhibition, subgrid-scale triggering energy, and
 334 stratiform instability in a toy tropical wave model. *J. Atmos. Sci.*, *57*(10),
 335 1515–1535.
- 336 Matsui, T., Chern, J.-D., Tao, W.-K., Lang, S., Satoh, M., Hashino, T., & Kubota,
 337 T. (2016). On the land–ocean contrast of tropical convection and micro-
 338 physics statistics derived from trmm satellite signals and global storm-resolving
 339 models. *Journal of Hydrometeorology*, *17*(5), 1425–1445.
- 340 Pendergrass, A. G., Knutti, R., Lehner, F., Deser, C., & Sanderson, B. M. (2017).
 341 Precipitation variability increases in a warmer climate. *Scientific reports*, *7*(1),
 342 17966.
- 343 Raymond, D., Fuchs, Z., Gjorgjievska, S., & Sessions, S. (2015). Balanced dynamics
 344 and convection in the tropical troposphere. *J. Adv. Model Earth Sys.*, *7*, 1093-
 345 1116. doi: 10.1002/2015MS000467
- 346 Robinson, F., Sherwood, S., Gerstle, D., Liu, C., & Kirshbaum, D. J. (2011). Ex-
 347 ploring the land–ocean contrast in convective vigor using islands. *Journal of*
 348 *the Atmospheric Sciences*, *68*(3), 602–618.
- 349 Seneviratne, S. I., Wilhelm, M., Stanelle, T., van den Hurk, B., Hagemann, S., Berg,
 350 A., . . . others (2013). Impact of soil moisture-climate feedbacks on cmip5 pro-
 351 jections: First results from the glace-cmip5 experiment. *Geophysical Research*
 352 *Letters*, *40*(19), 5212–5217.
- 353 Sherwood, S. C., & Huber, M. (2010). An adaptability limit to climate change
 354 due to heat stress. *Proceedings of the National Academy of Sciences*, *107*(21),
 355 9552–9555.
- 356 Sobel, A., Held, I., & Bretherton, C. (2002). The ENSO Signal in Tropical Tropo-
 357 spheric Temperature. *J. Climate*, *15*(18), 2702-2706.
- 358 Sobel, A. H., & Bretherton, C. S. (2000). Modeling tropical precipitation in a single
 359 column. *J. Climate*, *13*(24), 4378–4392.

- 360 Taylor, K. E., Stouffer, R. J., & Meehl, G. A. (2012). An overview of cmip5 and the
361 experiment design. *Bull. Am. Meteorol. Soc.*, *93*(4), 485–498.
- 362 Williams, E., & Renno, N. (1993). An analysis of the conditional instability of the
363 tropical atmosphere. *Monthly Weather Review*, *121*(1), 21–36.